



## ORIGINAL ARTICLE

# Comparative interactome mapping of Tau-protein in classical and rapidly progressive Alzheimer's disease identifies subtype-specific pathways

Abrar Younas<sup>1,2,3</sup> | Neelam Younas<sup>1,2</sup>  | Muhammad Javed Iqbal<sup>4</sup> |  
Isidre Ferrer<sup>5</sup>  | Inga Zerr<sup>1,2</sup>

<sup>1</sup>National Reference Center for Surveillance of TSE, Department of Neurology, University Medical Center Göttingen, Göttingen, Germany

<sup>2</sup>German Center for Neurodegenerative Diseases (DZNE), Göttingen, Germany

<sup>3</sup>Department of Biological Sciences, Faculty of Sciences, University of Sialkot, Sialkot, Pakistan

<sup>4</sup>Department of Biotechnology, Faculty of Sciences, University of Sialkot, Sialkot, Pakistan

<sup>5</sup>Department of Pathology and Experimental Therapeutics, University of Barcelona, Hospitalet de Llobregat, Spain

## Correspondence

Dr Neelam Younas, University Medical Center Göttingen, National Reference Center for Surveillance of TSE, Department of Neurology, Robert-Koch str. 40, 37075 Göttingen, Germany.  
Email: [neelam.younas@med.uni-goettingen.de](mailto:neelam.younas@med.uni-goettingen.de)

## Abstract

**Aims:** Tau is a key player in Alzheimer's disease (AD) and other Tauopathies. Tau pathology in the brain directly correlates with neurodegeneration in AD. The recent identification of a rapid variant of AD demands an urgent need to uncover underlying mechanisms leading to differential progression in AD. Accordingly, we aimed to dissect the underlying differential mechanisms of toxicity associated with the Tau protein in AD subtypes and to find out subtype-dependent biomarkers and therapeutic targets.

**Methods:** To identify and characterise subtype-specific Tau-associated mechanisms of pathology, we performed comparative interactome mapping of Tau protein in classical AD (cAD) and rapidly progressive AD (rpAD) cases using co-immunoprecipitation coupled with quantitative mass spectrometry. The mass spectrometry data were extensively analysed using several bioinformatics approaches.

**Results:** The comparative interactome mapping of Tau protein revealed distinct and unique interactors (DPYSL4, ARHGEF2, TUBA4A and UQCRC2) in subtypes of AD. Interestingly, an analysis of the Tau-interacting proteins indicated enrichment of mitochondrial organisation processes, including negative regulation of mitochondrion organisation, mitochondrial outer membrane permeabilisation involved in programmed cell death, regulation of autophagy of mitochondrion and necroptotic processes, specifically in the rpAD interactome. While, in cAD, the top enriched processes were related to oxidation–reduction process, transport and monocarboxylic acid metabolism.

**Conclusions:** Overall, our results provide a comprehensive map of Tau-interacting protein networks in a subtype-dependent manner and shed light on differential functions/pathways in AD subtypes. This comprehensive map of the Tau-interactome has provided subsets of disease-related proteins that can serve as novel biomarkers/biomarker panels and new drug targets.

Abrar Younas and Neelam Younas, Equal contribution.

This is an open access article under the terms of the [Creative Commons Attribution-NonCommercial-NoDerivs](https://creativecommons.org/licenses/by-nc-nd/4.0/) License, which permits use and distribution in any medium, provided the original work is properly cited, the use is non-commercial and no modifications or adaptations are made.

© 2024 The Authors. *Neuropathology and Applied Neurobiology* published by John Wiley & Sons Ltd on behalf of British Neuropathological Society.

## KEYWORDS

biomarkers, drug targets, interactome, mass spectrometry, rapidly progressive Alzheimer's disease, Tau

## INTRODUCTION

Tau protein is a crucial player in several neurodegenerative disorders. Pathogenic variants of the Tau gene (*MAPT*) lead to neurodegenerative disorders like frontotemporal dementia (FTDP) [1, 2]. In Alzheimer's disease (AD), the Tau protein accumulates in the form of neurofibrillary tangles (NFTs) in the neurons and becomes toxic. Tau pathology in the brain directly correlates with neurodegeneration in AD [3].

AD is a complex, heterogeneous and multifactorial malady with various clinicopathological subtypes [4]. The classic form of AD (cAD) exhibits a slowly progressive cognitive decline with prominent memory loss and an approximate eight-year survival time after the onset of clinical symptoms [5–8]. In addition to classical AD cases, recently a variant of AD named rapidly progressive AD (rpAD) has been identified [8–11]. Rapidly progressive AD cases exhibit a very rapid decline in cognitive status [12], different biomarker profiles [13, 14] and distinct amyloid-beta ( $A\beta$ ) [15–17] and Tau strain [8, 11] profiles. These studies suggest a distinct pathological cascade in patients with rpAD. However, the underlying mechanism(s) of the fast progression of the disease is still enigmatic. An understanding of disease subtype-specific molecular perturbations is urgently required for early discrimination of rpAD from cAD, for the diagnostic and clinical management of patients and, possibly, for the development of customised and focused therapies.

AD is a dual proteinopathy ( $A\beta$  and Tau pathology). However, the load of misfolded Tau protein (Tau pathology) seems to be the critical factor in determining cognitive decline [18, 19]. Like all proteins in a cell, the precise functions and localisation of Tau protein are dependent on its interaction with many other cellular proteins [20, 21]. Alterations in the Tau interactome, including new disease-associated interactions, may initiate or aggravate Tau pathology or could be protective by reducing Tau pathological species and/or inflammation [22]. In addition, different conformations of Tau protein influence its interactions and functions [23].

Very recently, distinct misfolded conformers of Tau protein have been discovered in rpAD [11] implying concomitantly altered Tau interactions, which may lead to different disease mechanisms [11]. Mapping of the Tau interactome, particularly the investigation of the interactome of pathological Tau strains, can be an excellent way to delineate disease subtype-specific mechanisms. The interactions of Tau protein are influenced by many factors, for example, cellular localisation, isoform, aggregation status, conformation and the presence of various post-translational modifications. Thus, analysis of strain- and disease subtype-specific Tau interactomes can provide a unique opportunity to uncover differential disease mechanisms, subtype-specific novel biomarkers, and therapeutic targets.

Previously, investigations of the Tau interactome have been carried out in the context of AD (with balanced 3R/4R Tau or localised proteomics in AD post-mortem human tissue) [24–27] or in cellular models expressing Tau variants linked with a rare familial form of FTLD (P301L or V337M) [28–30]. However, comparative in-depth

## Key points

- Biological processes related to mitochondrial organisation (and its dynamics) and necroptotic processes were over-represented in rpAD.
- Oxidation–reduction and transport were overrepresented in the cAD-Tau interactome.
- Disease subtype-specific subsets of proteins (unique and differentially abundant interactors) provide new targets for the development of subtype-dependent biomarkers and therapeutic targets.

Tau interactome mapping in subtypes of AD is still missing. Thus, to the best of our knowledge, the current study is the first that aimed at this primary objective to generate an in-depth inventory of subtype-specific Tau interactome maps in cAD and rpAD cases.

Here, comparative Tau interactome mapping enabled us to quantitatively compare complex protein–protein interactions of cAD with rpAD in the human brain frontal cortex. The current study generated a comprehensive map of Tau-linked protein networks. The identified proteins could be targeted for therapeutic interventions to slow down Tau-mediated disease progression. Unique interactors can be utilised as subtype-specific novel biomarkers and therapeutic targets.

## MATERIALS AND METHODS

## Ethics statement

Frontal cortical samples from subjects with cAD and rpAD were obtained from prion surveillance centres in Spain (according to legislation, Ley de la Investigación Biomédica 2013 and Real Decreto Bio-bancos, 2014) and Germany (No. 24/8/12) [8]. Ethics approvals were obtained from the local Ethical Committees of the University Medical Centre, Göttingen, and Institute of Neuropathology Brain Bank (HUB-ICO-IDIBELL Biobank) and Biobank of Hospital Clinic-IDIBAPS Spain. All the procedures were carried out following ethics regulations.

## Sample collection and processing

Frontal cortical samples of AD subtypes (cAD, rpAD) were processed as previously [8]. One-centimetre thick tissue slices from one hemisphere were snap-frozen for biochemical analysis. The second hemisphere was used for neuropathological assessment to validate the

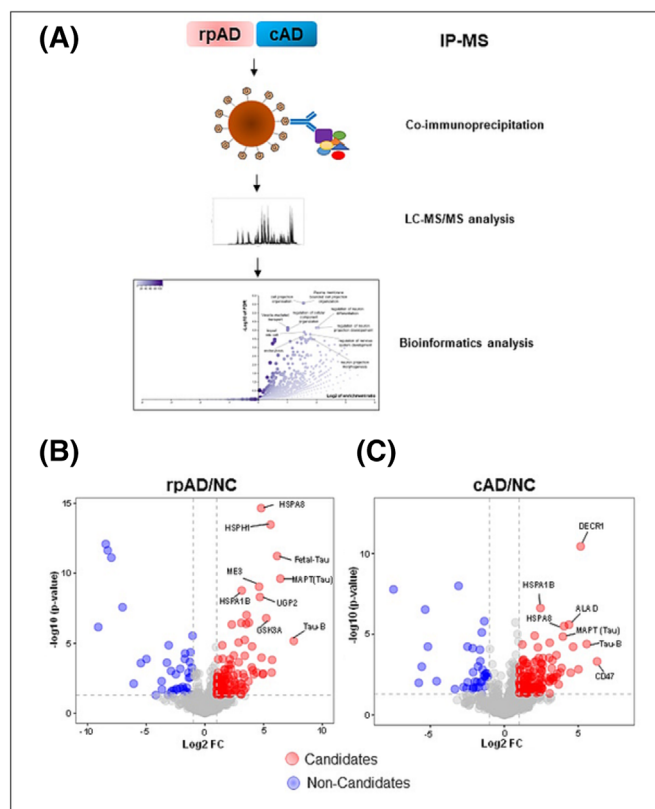


**FIGURE 1** Interactome mapping of Tau protein using co-immunoprecipitation and mass spectrometry analysis. (A) An overview of the methodology. (B & C) Volcano plots show significantly enriched proteins in both cAD and rpAD in comparison with negative control (NC) (Welch's *t*-test *p*-value < 0.05 and FC ≥ 2). The Y-axis shows the  $-\log_{10}$ -*p*-values and the X-axis shows the  $\log_2$  (FC) of the proteins. The dashed lines indicate Welch's *t*-test cut-off, the data points above the dashed lines represent proteins having a *p*-value < 0.05 and FC ≥ 2 as significant hits (candidates), which are depicted in red and blue (for depleted: non-candidates).

clinical diagnosis. The neuropathological workup of all the samples is described in detail by Hernandez et al. [31]. All the subjects were confirmed by neuropathological investigation of 25 regions of the cerebral cortex, cerebellum, diencephalon, thalamus and brainstem [31]. Haematoxylin and eosin, Klüver–Barrera and immunohistochemistry (for  $\beta$ -amyloid, phosphorylated Tau,  $\alpha$ -synuclein, TDP 43, glial fibrillary acidic protein, ubiquitin, p62 and microglial-specific markers) were accomplished [31]. The selection of rpAD samples was performed according to the definition of rpAD [32]. Typical AD is denoted as classical AD (cAD) in the current study (Suppl. Figure 1A).

### Tissue lysis and co-immunoprecipitation

Tissue lysis was accomplished as described before [8]. Briefly, 10% w/v tissue homogenates were prepared (1% Triton X-100, 50mM Tris–HCl [pH 8], 1mM DTT, and 0.5% CHAPS) on ice with phosphatase and protease inhibitors (Roche) followed by incubation at 4°C for

overnight to settle down foam and debris. The tissue homogenates were cleared of debris by centrifugation at 14,000 rpm for 30 min at 4°C. Co-immunoprecipitation was done with anti-Tau antibody (Tau-5, #ab80579) using protein G magnetic Dynabeads (Invitrogen), according to the manufacturer's instructions with corresponding negative controls (Mouse IgG isotype control, #31903). For co-immunoprecipitation, 500  $\mu$ g total protein was used as an input. In total, we performed eight co-immunoprecipitations. Three biological replicates (three different individuals) were co-immunoprecipitated from each group (three subjects with cAD and three subjects with rpAD) with a representative negative control from each group separately. Each biological replicate was run three times in the mass spectrometer (technical replicates, *n* = 24). Data was transferred to Perseus software (V 1.6.0.7) [33, 34] and log-transformed followed by statistical analysis (details are in Section 2.6).

### Immunoblotting analysis

Immunoblotting analysis was accomplished as described previously [35]. Briefly, total tissue extracts (50  $\mu$ g) or co-immunoprecipitates were electrophoresed onto 4–12% Bis-Tris gels (NuPAGE™ 4–12% Bis-Tris Protein Gels, Invitrogen). The expression analysis of target proteins was carried out by overnight exposure to primary antibodies including anti-Tau monoclonal antibody (Tau-5, 1:1000, #Ab80579), anti-Tau mAb (E178\_phosphoS396, 1:1000, #ab32057), anti-phospho Tau mAb (T231, 1:1000, #ab226492), and anti-GAPDH antibody (1:1000, # G8795) at 4°C. Images were acquired using Chemi-Doc (Bio-Rad) by developing membranes into enhanced chemiluminescence solution. The band intensities were calculated using Image Lab software (3.0.1).

### Mass spectrometry analysis

Protein samples were run onto 4–12% NuPAGE Novex Bis-Tris Mini gels (Invitrogen) for a length of ~1 cm (one thick band). The resulting gels were stained with Coomassie brilliant blue stain. The thick protein bands were cut out of the gels, sliced, and processed for reduction (with dithiothreitol: DTT), alkylation (with iodoacetamide: IAA), and finally digested with trypsin overnight. The resulting peptides were isolated from the gel. The mixture was dried using a Speedvac and stored at –20°C for mass spectrometry analysis.

Digested proteins (tryptic peptides) were analysed using a nano-flow chromatography system (Dionex U3000 nanoRSLC) connected to a tribrid mass spectrometer (Orbitrap Fusion) equipped with a NanoFlex ion source and controlled by Excalibur software v3.4 (all Thermo Fisher Scientific, Dreieich, Germany). In brief, the loading buffer (2% acetonitrile, 0.1% formic acid in water) was used to dissolve to a final concentration of 100 ng/ $\mu$ L. For all the analyses 400 ng of digested proteins were enriched on a pre-column (0.15 mm ID  $\times$  20 mm, Reprosil-Pur120 C18-AQ 5  $\mu$ m, Dr Maisch, Ammerbuch-Entringen, Germany) and separated on an analytical RP-

C18 column (0.075 mm ID × 200 mm, Reprosil-Pur 120 C18-AQ, 1.9 µm, Dr Maisch) using a 37 min linear gradient of 5–35% acetonitrile/0.1% formic acid (v:v) at 300 nl/min.

MS/MS data were obtained employing data-independent acquisition (DIA) using 40 variable-size windows [36] across the 350–1250 m/z range. The fragments were generated using staggered NCE settings (26/28/30%) for charge state 3+ at a resolution setting of 60,000 FWHM, an AGC target of 1\*10e6, and a maximum fill time of 54 ms. Three technical replicates were run for all the samples.

Identification of the proteins, construction of a spectral library, and DIA peak integration were accomplished in Spectronaut Software v16 (Biognosys, Schlieren, Switzerland) [37]. Peptides and proteins were identified using the in-built Pulsar algorithm at default settings. The combined qualitative analyses were searched against the UniProtKB human reference proteome (revision 04-2021) supplemented with a set of 52 known common laboratory contaminants to identify peptide-to-sequence matches, peptides and proteins at false discovery rates (FDR) of 1%, respectively. Peptide identifications were transcribed into an annotated hybrid MS/MS spectral library using all DDA and DIA runs.

DIA peak integration was performed in Spectronaut using default parameters. Dynamic retention time correction was performed using endogenous peptides, followed by peak area extraction using the spectral library at a critical FDR of 1%. The extracted peak areas were summed to peptide and finally protein area values/replicate. The resulting values were statistically evaluated. DIA quantification was performed using up to six fragments per peptide, up to 10 peptides per protein, dynamic retention time alignment and dynamic mass recalibration followed by quartile normalisation, at 1% FDR. Global data

imputation was performed for the final results table. Raw data from MS/MS with its identification parameters is detailed in Suppl. Table 1 including the number of stripped sequences identified, no. of precursors identified, their *p*-values and corresponding *c*-score ((discriminant score used for the FDR: Spectronaut's C score).

## Differential enrichment analysis of the interactome

Raw data from mass spectrometry analysis was transferred to Perseus software (V 1.6.0.7) [33], followed by log transformations. In total, 2164 proteins were identified and quantified. Firstly, to measure the variation between replicates, we calculated %CV (percent coefficient of variance) for all the proteins. For both groups, this was below 10% (Suppl. Figure 1B). Furthermore, we also calculated Pearson correlation coefficients of different replicates of the same sample (technical replicates); these were between 0.904 and 0.954, indicating a strong correlation among different replicates of the same sample (Suppl. Figures 3 & 4). The Pearson correlation coefficients between interactome profiles from biological replicates were between 0.830 and 0.96, indicating a high degree of correlation and good reproducibility (Suppl. Figure 5). For statistical comparisons in Perseus software, representative negative controls were grouped, and biological and technical replicates were combined. To identify proteins that were significantly enriched in the target groups (cAD and rpAD in comparison with negative controls), we performed a Welch's *t*-test, where fold change (FC) for all comparisons' thresholds was set at ≥2 and a *p*-value <0.05 for significance (Suppl. Table 1). In this approach, the analysis was not corrected for the multiplicity given the exploratory nature of the study [52].

**TABLE 1** A list of interactors that were exclusively enriched in either cAD or rpAD-Tau interactome.

Group	Gene names	Uniprot-ID	Relevance with AD	Count	References
cAD	TPI1	TPIS_HUMAN	Predicted as a new biomarker of AD [38]	2	[28, 39]
	UQCRFS1P1	UCRIL_HUMAN	Differentially expressed in PD [40]	-	
	BSG	A0A087WUV8_HUMAN	Affects Aβ accumulation [41]	1	[28]
	UQCRC2	QCR2_HUMAN	Down-regulated in the early onset AD [42]	2	[27, 28]
	RPS27A	RS27A_HUMAN	Identified as one of the Hub genes in AD [43]	4	[26, 28–30]
	PGRMC1	PGRC1_HUMAN	-	-	
	ENO2	ENOG_HUMAN	Down-regulated in AD [44, 45]	2	[27, 28]
	HADHA	HOYFD6_HUMAN	Decreased in AD [46]	3	[28, 30, 47]
	ANXA6	ANXA6_HUMAN	-	2	[28, 48]
rpAD	FARSB	SYFB_HUMAN	-	3	[27–29]
	TUBA4A	TBA4A_HUMAN	Increased in rpAD and cAD [49]	3	[27–29]
	SEC24C	G5EA31_HUMAN	Increased in rpAD in comparison with DFTL [49]	1	[28]
	DPYSL5	DPYL5_HUMAN	Reduced in rpAD vs cAD [49]	1	[28]
	DPYSL4	DPYL4_HUMAN	Presymptomatic biomarker of AD [50]; Increased in rpAD vs SVD [49]	1	[28]
	ARHGEF2	A0A5F9ZI21_HUMAN	Increased in rpAD vs cAD [51]	-	
	GLS	GLSK_HUMAN	Differentially regulated in rpAD [49]	-	
	HSPA12A	A0A1B0GTF3_HUMAN	-	3	[24, 27, 28]

The candidate interactors were compared with the literature and out of 179 candidate interactors, 135 proteins were already reported as Tau interactors in the literature (Suppl. Table 1). Given the exploratory nature of the present study and the high similarity of our interactome with the previous interactomes, the candidate interacting partners originating from this approach were used for subsequent functional enrichment analyses.

## Bioinformatics analyses

Proteins that were significantly enriched in a target group over IgG-IP isolates (Welch's *t*-test, *p*-value <0.05, FC ≥ 2) were considered as putative interacting partners of Tau protein. Labelled volcano plots were calculated using Perseus software and were plotted using R (version 3.4.3). Here, FC was transformed to log2 scale, so that the data was centred on zero, and *p*-values were transformed into  $-\log_{10}$ .

To do a comparison of interactors between cAD and rpAD, statistically significant interacting partners of Tau protein in each group were uploaded to explore the similar and unique proteins by Venny (V2.1.0). To assess the interconnectivity of the candidate interactors in the form of a network, a protein-protein interaction network was built using STRING (V11.5).

Next, we performed differential abundance analysis in subtypes of AD. The proteins that were not significantly different between iso-type and co-IP were removed and then levels of the remaining interactors were compared between rpAD and cAD. A list of significant interactors that were differentially abundant in both subtypes is detailed in Suppl. Table 1. Sixty proteins were significantly abundant in rpAD in comparison with cAD (Figure 2A, Suppl. Table 1). Seventy-three proteins were significantly abundant in cAD in comparison with rpAD (Figure 2A, Suppl. Table 1).

To identify the biological and functional significance of Tau-interactome, we performed functional enrichment analysis using the Web-based Gene Set Analysis Toolkit (WebGestalt) [53]. Initially, all statistically significant interacting partners of Tau protein in each group were used for enrichment analysis to get a complete functional profile in both groups. The enrichment analysis was corrected for background. Overrepresentation analysis was performed in the domain of biological process (BP). The output from WebGestalt gives two major sections "GO Slim summary" and enrichment results. Then, enrichment analysis was performed using only unique interacting partners in both subtypes to find out specific biological pathways enriched in a subtype-dependent manner.

## Statistical analysis

The results in the current study were obtained from at least three independent experimental replicates. Immunoblotting images were analysed using GraphPad Prism (9. 5.1). All the statistical tests are described as mean ± standard error of the mean. The data from mass spectrometry was processed and analysed using the Perseus software.

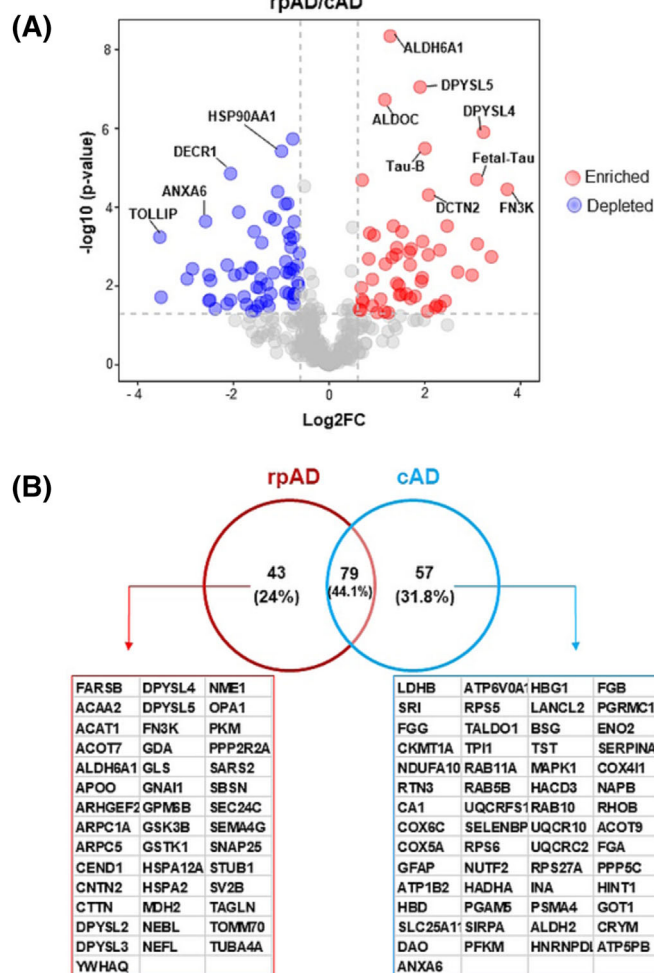


**FIGURE 2** Comparison between cAD and rpAD-Tau-interactome. (A) A volcano plot shows significantly abundant proteins in rpAD in comparison with cAD. For differential abundance analysis, the significant interactors were compared using Welch's *t*-test between rpAD and cAD. The Y-axis shows the  $-\log_{10}(p\text{-value})$  and the X-axis shows the  $\log_2(FC)$  of the proteins. The dashed lines indicate Welch's *t*-test cut-off, the data points above the dashed lines represent proteins having a *p*-value <0.05 and FC ≥ 2 as significantly abundant (red) or depleted (blue). (B) A Venn diagram shows shared and unique interactors between cAD and rpAD. The significantly enriched interactors over negative control were compared to find out shared and unique interactors between rpAD and cAD.

Statistical significance was achieved at a *p*-value <0.05. Figures were processed using Inkscape (0.91).

## RESULTS

### Co-immunoprecipitation and mass spectrometry analysis

Different strains of Tau protein influence protein interactions and functions [54]. Accordingly, to enrich pathophysiological interactions of Tau protein, we performed comparative interactome mapping of



total-Tau (Tau-5, mouse) in subtypes of AD (cAD and rpAD) using co-immunoprecipitation (CO-IP) combined with quantitative mass spectrometry analysis (Figure 1A). Immunoblotting analysis (Rabbit anti-Tau-E178, Phospho S396) of the immunoprecipitates showed enrichment of Tau protein in human brain frontal cortices in both groups (Suppl. Figure 2A & B). Overall, there were no significant differences in the levels of total Tau between both subtypes of AD (Suppl. Figure 2C & E).

There was differential phosphorylation at S396 and T231 in rpAD cases in comparison with cAD cases. The levels of phospho S396 were significantly decreased in rpAD cases when compared with cAD cases (Suppl. Figure 2D & G). For Phospho-T231, there were no significant differences, although an increasing trend was observed for rpAD cases (Suppl. Figure 2C & F). The signal of Tau (Phospho S396) is weaker in rpAD co-immunoprecipitates (Suppl. Figure 2A), as the general expression of this phosphorylation site is significantly decreased in rpAD cases, in comparison with cAD cases (Suppl. Figure 2B, D & G).

In total, we identified 179 high-confidence (Welch's *t*-test,  $p < 0.05$ ,  $FC \geq 2$ ) Tau interactors that were significantly enriched in target groups in comparison with isotype controls (Figure 1B). A complete list of all the significantly enriched interactors with their individual *p*-values and FC is described in the Suppl. Table 1. The identification of numerous Tau interactors with high confidence in the current study was a result of our stringent Co-IP-MS approach. Triplicate biological replicates from each group (three classical AD and three rpAD cases with representative negative controls) were run three times in the mass spectrometer.

As expected, Tau protein (MAPT) was significantly enriched in both groups in comparison with isotype control (Figure 1B, Suppl. Table 1). Interestingly, three isoforms of Tau protein (Isoform Fetal-Tau, Isoform Tau-B, and Isoform Tau-C of Microtubule-associated protein Tau) were also significantly enriched in both groups in comparison with isotype control (Suppl. Table 1).

The candidate interactors were compared with the literature, and out of 179 candidate interactors, 135 proteins were already reported as Tau interactors in the literature (Suppl. Table 1). We also curated the bait protein (as Tau, phosphorylated Tau, or mutated Tau) of our interactome candidates from the literature, and whether these candidate interacting proteins localise in the neurofibrillary tangles and are altered in them or not. All these comparisons are detailed in the Suppl. Table 1.

According to the emerging field of 'network medicine', the interactomes can be interpreted as network maps and perturbations in these networks could reveal common and unique molecular themes as a result of a pathological condition [55]. To estimate the interconnectivity of the candidate interacting partners in the form of a network, we mapped the interaction partners using the STRING (Search Tool for the Retrieval of Interacting Genes/Proteins) database in both subtypes of AD (Supplementary Figures S6 & S7). Most of the candidate interaction partners were associated in the protein–protein interaction network at a medium confidence score (score  $\geq 0.4$ ) in both

subtypes of AD, which were associated with distinct functional outcomes (Figures 4–6).

## Comparison between cAD and rpAD interactome

To determine the differences between cAD and rpAD interactomes, significantly enriched candidate interactors were compared using Venny (2.1.0). Seventy-nine proteins were similar between both groups. The similar and unique proteins between classical AD and rapidly progressive AD Tau-interactomes are shown in Figure 2B, Suppl. Table 1. There were 57 proteins that passed our cut-off criteria (Welsch's *t*-test *p*-value  $< 0.05$  and  $FC \geq 2$ ) and were uniquely enriched in the cAD-Tau interactome. Forty-three candidate interactors reached the significance threshold in rpAD-Tau interactome according to the above criteria. Some of these unique candidate interactors were also present in the other group but did not pass the inclusion criteria (Figure 2B, Suppl. Table 1). Next, we screened out real unique interactors (those interactors that were exclusively enriched in one group and were negatively enriched in the other group). Table 1 shows details of these real unique interactors from both groups and their relevance with AD.

Next, we performed differential abundance analysis in subtypes of AD. The proteins that were not significantly different between isotype and co-IP were removed and then levels of the remaining interactors were compared between rpAD and cAD. A list of significant interactors that were differentially abundant in both subtypes is detailed in Suppl. Table 1. Sixty proteins were significantly abundant in rpAD in comparison with cAD (Figure 2A, Suppl. Table 1). Seventy-three proteins were significantly abundant in cAD in comparison with rpAD (Figure 2A, Suppl. Table 1). There were no significant differences between MAPT (Tau) protein between cAD and rpAD (Figure 3A). Strikingly, isoforms of Tau-protein (Isoform Fetal-Tau, Tau-B and Tau-C of MAPT) were significantly abundant in rpAD in comparison with cAD (Figure 3B–D). Some of the other differentially abundant proteins in rpAD in comparison with cAD were DPYSL4 and ARHGEF2 (Figure 3E & F). The proteins NUTF2, COX5A and COX6C were significantly abundant in cAD in comparison with rpAD (Figure 3G–I, Suppl. Table 1).

## Specific enrichment of biological processes related to transport and Rab protein signal transduction in the cAD Tau-interactome

To understand systematically the functional significance of the identified interactome, we performed a functional enrichment analysis of the significant interactors in cAD Tau-interactome.

Firstly, we performed an over-representation analysis (ORA) using the WEB-based Gene Set Analysis Toolkit (WebGestalt) [53]. GO slim summary from WebGestalt shows protein distribution of the interactome in GO domains 'biological process', 'molecular function' and 'cellular component' (Figure 4A). Enrichment analysis in the domain of 'Biological Process' revealed the 'establishment of

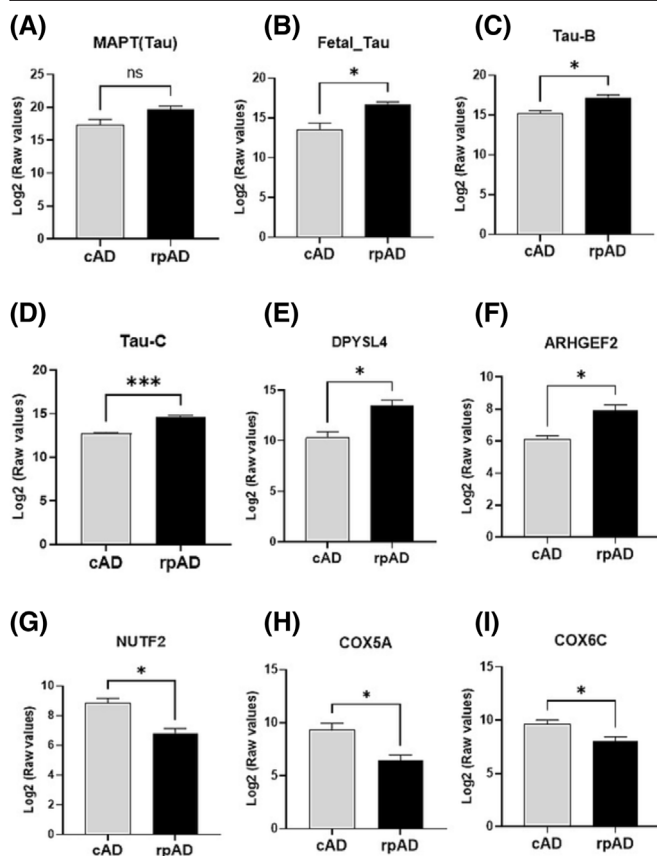


**FIGURE 3** Differentially abundant candidate interactors in cAD and rpAD-specific interactomes. Few examples of differentially abundant protein interactors are shown. (A–F) Proteins significantly abundant in rpAD in comparison with cAD. (G–I) The candidate interactors significantly abundant in cAD, in comparison with rpAD. The raw intensity values of technical replicates ( $n = 18$ ) from mass spectrometry analysis were average for all biological replicates ( $n = 6$ , 3 biological replicates from each group) and the statistical tests (Welch's  $t$ -test) were applied in the GraphPad prism (9.5.1) with significance at \* $p < 0.05$ , \*\* $p < 0.01$ , \*\*\* $p < 0.001$ .

localisation (FDR =  $2.51E-05$ ), 'transport (FDR =  $2.51E-05$ )' and 'Rab protein signal transduction ( $1.05E-04$ )' as the most enriched functional terms (Figure 4B). The top 10 enriched biological processes with their corresponding genes and statistical parameters are detailed in the Supplementary Table S2.

Next, we took the list of our Tau-interacting proteins that were significantly abundant in cAD Tau-interactome in comparison with rpAD Tau-interactome and performed functional enrichment analysis to identify specific and unique biological functions linked with Tau-interactome in this subtype of AD.

We performed GO term enrichment analysis in the domain of BP using WebGestalt. This analysis showed 'oxidation-reduction process (22 proteins)', 'homeostatic process (23 proteins)', 'monocarboxylic acid metabolic process (14 proteins)', 'transport (45 proteins)' and 'establishment of localisation (45 proteins)' as the most enriched clusters (Figure 6B) in cAD. The top 10 enriched biological processes with their proteins are listed in the Supplementary Table S2.

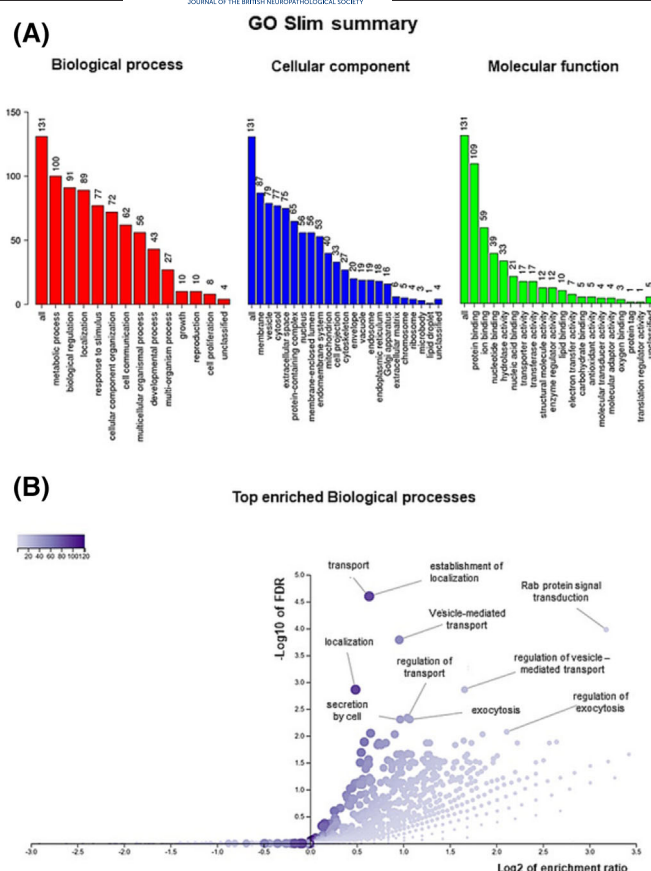


**FIGURE 4** Significantly enriched GO biological processes in classical AD (cAD) Tau-interactome. (A) GO slim summary of interacting partners. A red, blue and green bar represents the distribution of proteins in GO-terms biological process, cellular component and molecular function, respectively. (B) A volcano plot shows enriched biological processes in the cAD Tau-interactome. The top 10 enriched terms are labelled. The volcano plot shows log10 of FDR against the enrichment ratio on a log2 scale. Terms with smaller enrichment ratios, for example, below one will be plotted as negative enrichment on the log2 scale. Significant categories are near the upper corners. The colour and size of the dot are relative to the size of the category.

### Enrichment of biological processes related to mitochondrial organisation and import into the cell in the rpAD Tau-interactome

To explore in detail if a particular biological process was significantly enriched in the subset of proteins that preferentially co-isolated with Tau protein in rapidly progressive AD, we performed an over-representation analysis using WebGestalt [53]. GO slim summary from WebGestalt shows the protein distribution of the interactome in three GO domains (Figure 5A). Enrichment results of the GO-term biological process revealed 'plasma membrane bounded cell projection organisation (FDR =  $2.67E-06$ )', 'regulation of neuron differentiation (FDR =  $7.24E-05$ )' and 'import into cell (FDR =  $1.74E-04$ )' as the most enriched terms in the rpAD Tau-interactome (Figure 5B, Suppl. Table S2). The top 10 enriched biological processes with their

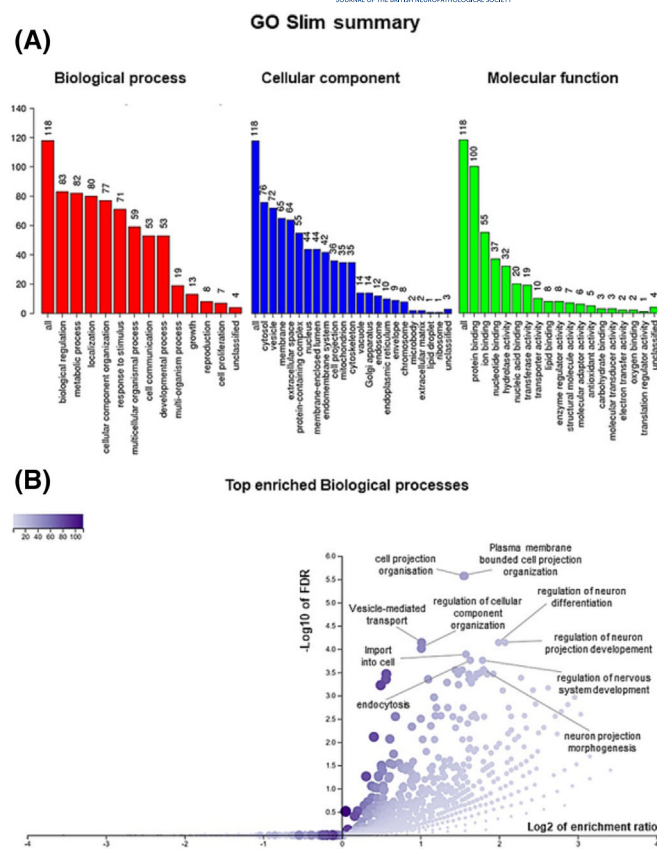


**FIGURE 5** Significantly enriched GO biological processes in rapidly progressive AD (rpAD) Tau-interactome. (A) GO slim summary of interacting partners. A red, blue and green bar represents the distribution of proteins in GO-terms biological process, cellular component and molecular function, respectively. (B) A volcano plot shows enriched biological processes in the rpAD Tau-interactome. The top 10 enriched terms are labelled. The volcano plot shows  $\log_{10}$  of FDR against the enrichment ratio on a  $\log_2$  scale. Terms with smaller enrichment ratios, for example, below one are plotted as negative enrichment on a  $\log_2$  scale. Significant categories are near the upper corners. The colour and size of the dot are relative to the size of the category.

corresponding genes and statistical parameters are detailed in the Supplementary Table S2.

To further identify unique biological processes enriched in the interaction network in rpAD-Tau interactome, we took out the list of significantly abundant proteins in rpAD in comparison with cAD and performed functional enrichment analysis. This analysis identified two predominant themes: Mitochondrion organisation and necroptotic processes (Figure 6A). Notably, the results showed enrichment of 'regulation of mitochondrion organisation (MAPT; DNM1L; GSK3A; PPIF; YWHAQ; CTTN; ACAA2)' 'small molecule catabolic process (GLS; GSK3A; BDH2; ALDH6A1; ALDOC; ALDOA; ACAA2; ACAT1; PKM; HSD17B4)', 'regulation of protein complex assembly (MAPT; STUB1; DNM1L; STXBP1; ARHGEF2; PFN2; PTPN11; PPP3; CTTN; ARPC1A)', 'regulation of autophagy of mitochondrion (DNM1L; GSK3A; CTTN)' and 'necroptotic processes (DNM1L; ARHGEF2; PPIF)' as the most enriched clusters (Figure 6A) in rpAD. The top

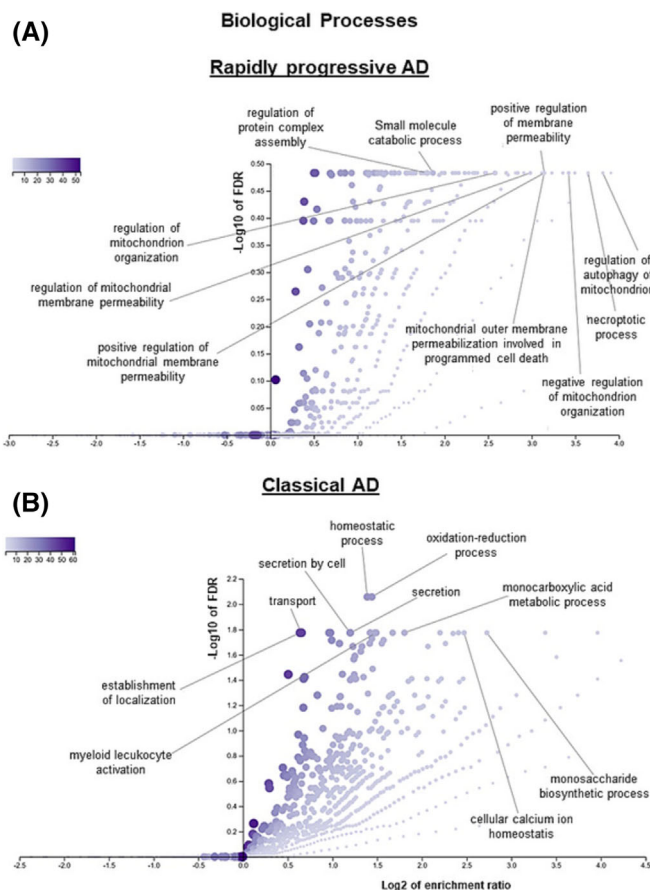


**FIGURE 6** Uniquely enriched biological processes in cAD and rpAD Tau-interactome. (A) The volcano plot shows specifically enriched biological processes in rpAD. The top 10 enriched terms are labelled. The volcano plot shows  $\log_{10}$  of FDR against the enrichment ratio on a  $\log_2$  scale. Significantly abundant interactors from rpAD were used for enrichment analysis. (B) The volcano plot shows specifically enriched biological processes in cAD. The top 10 enriched terms are labelled.

10 enriched biological processes with their corresponding proteins are listed in Supplementary Table S2.

## DISCUSSION

We used IP-MS to map the comparative interactome of pathological Tau protein in the human brain frontal cortical region in classical AD and rpAD to uncover disease subtype-specific mechanisms. The advance in the current work is an in-depth interactome mapping of AD subtypes, specifically the study of rapidly progressive AD.

We identified 179 Tau interactors that were significantly (Welsh's *t*-test, *p*-value < 0.05 and FC ≥ 2) enriched in a target group in comparison with isotype controls. Identification of numerous Tau-interactors with high confidence in the current study was a result of our stringent CO-IP-MS approach. Triplicate immunoprecipitates (three biological replicates) from each group were run three times in a mass spectrometer. Several known interactors were detected in our data set including the 14-3-3 protein family (14-3-3 protein eta, 14-3-3 protein theta,



14-3-3 protein beta/alpha, 14-3-3 protein gamma), heat shock cognate 71 kDa protein, and growth factor receptor-bound protein 2 [56], validating our data. Out of 179 candidate interactors, 135 proteins were already reported as interactors of Tau protein in the human brain or cellular models (Suppl. Table 1). Several novel interactors were identified in the current study (Suppl. Table 1). It should be noted that all the proteins may not be interacting directly with the Tau protein, but some proteins may be indirect interactors. The property of Tau protein to bind with several different groups of proteins, and thus playing so many roles in the cell, stems from Tau being present as six different isoforms [57], from its ability to be widely modified by post-translational modifications and terminal truncations, and its multitude interacting regions [58].

Total-Tau antibody was used for co-immunoprecipitation, which binds to both phosphorylated and non-phosphorylated Tau isoforms. A comparison with the literature revealed the interaction of our candidates with total-Tau, phospho-Tau and pathogenic variants of Tau (Suppl. Table 1), suggesting enrichment of both physiological and pathological interactors. The significant abundance of isoforms of Tau protein (Fetal-Tau, Tau-B and Tau-C) in rpAD cases in comparison with cAD in our data set, suggests the existence of a mixture of different predominant isoforms in rpAD cases. Recently, it has been reported that a spectrum of misfolded Tau conformers with distinct structural organisations and different seeding properties (range of conformational Tau strains) are present in rapidly progressive AD [11]. Furthermore, different trajectories of Tau accumulation and post-translational modifications have been reported in phenotypes of AD [59]. Differential abundance of Tau isoforms in subtypes of AD may have a role in the progression of the disease.

Enrichment of biological processes related to oxidation–reduction and energy production in cAD corroborates with the well-known involvement of Tau protein in oxidation–reduction and metabolic processes [60, 61] and indicates the reliability of our proteomics data. Other significantly enriched biological processes were transport (establishment of localisation) and Rab protein signalling in cAD. Previously, an impairment of the endo-lysosomal pathway has been associated with AD pathology [62].

Notably, the results showed enrichment of mitochondrial processes (negative regulation of mitochondrion organisation, positive regulation of membrane permeability of mitochondrion) and regulation of autophagy of mitochondrion exclusively in rpAD. Membranes of mitochondria are direct targets for toxic Tau species, particularly in synapses, where numerous mitochondria are present [28, 63]. Neurons are particularly vulnerable to mitochondrial abnormalities. Impairment in mitochondrial dynamics leads to dysfunction and loss of synapses. This loss of synapses is directly correlated with cognitive decline and ultimately leads to neuronal loss, starting from the entorhinal cortex and hippocampus to other areas of the cortex [64]. The altered binding of Tau protein to mitochondrial proteins due to FTDP-linked pathogenic variants impairs bioenergetics [28].

The biological process, vesicle-mediated transport, was enriched in both subtypes of AD. Neuronal cargoes cross a complex cytoskeleton to their specific destinations in the axon. Neurons rely on a well-

organised and efficient vesicular transport system including protein folding and sorting, transport vesicle organisation, delivery of these vesicles through the cytoskeleton to their target sites, and vesicle fusion/targeting [65]. Microtubule-associated proteins including Tau are a key component of these regulatory networks. Aberrant Tau phosphorylation can disrupt the targeting of critical cargoes to their specific destinations [66]. Recently, it has been reported that patients with rpAD contain ~80% misfolded four-repeat Tau (4R-Tau) and ~20% of misfolded 3R-Tau isoform with similar conformations [11].

Unique candidate interactors identified in subtypes of AD may serve as potential biomarkers and therapeutic targets. Triose phosphate isomerase 1 (TPI), a unique interactor enriched in cAD-Tau interactome (Table 1) has been recently predicted to be a new biomarker for AD [38]. TPI has been shown to interact with Tau protein in AD [39], and its gene expression is reduced in AD in a cell-type-specific manner [67]. Additionally, it has been reported that TPI protein interacts directly with the Parkin protein (a ubiquitin ligase) and potentially affects mitochondrial function [68]. Another protein, Annexin A6 was also exclusively enriched in cAD cases and was significantly abundant in cAD in comparison with rpAD. Annexin A6 is very important in forming repair caps and membrane repair in the neurons [69]. Exclusive enrichment of this protein in cAD highlights a potential disturbance in this crucial repair mechanism in rpAD that may aggravate the disease. Differential abundance of COX5A and COX6C in cAD Tau-interactome suggests distinct regulation of these proteins in subtypes of AD. Previously, COX5A has been implicated in memory impairment linked with the ageing brain [70] and decreased expression of COX6C at the transcriptional level has been reported in AD cases [71]. Abnormal cytoplasmic accumulation of nuclear transport factor 2 (NUTF2; Figure 3G) and its aggregation in the hippocampal neurons of a subset of AD cases have been reported [72, 73]. Interestingly, all of the above-discussed proteins also localise in NFTs in AD [24]. Their differential abundance in cAD and localisation in NFTs indicate the different compositions of NFTs in subtypes of AD pathology.

Dihydropyrimidinase-related protein 4 (DPYSL4), a cytoskeletal regulator, was significantly more abundant in rpAD in comparison with cAD, in our data. Recently, it has been identified as a presymptomatic marker in the 3xTG-AD-like mouse model [50]. Interestingly, Dihydropyrimidinase-related protein 4 is increased in high-density fractions in rpAD cases in comparison with small vessel disease (SVD) [49]. Rho guanine nucleotide exchange factor 2 (ARHGEF2) was exclusively enriched in rpAD Tau-interactome, as well. This protein is increased in rpAD in comparison with cAD, in high-density fractions from rpAD cases [49]. Increased disintegration of the cytoskeleton has been reported in rpAD cases in comparison with cAD cases [49], which corroborates our results. In the present study, because of the limited availability of human brain material, new interactors of Tau protein identified in subtypes of AD were not validated. Future investigations are required to validate new targets and to explore their biomarker potential in a subtype-dependent manner.

Altogether, the results from the current study provide new insights into the PPIs, biological functions, and roles of Tau protein in

AD subtypes. Identification of differential biological processes and pathways in subtypes of AD suggests that protein–protein interactions of Tau protein influence its aggregation dynamics and toxicity, contributing to different strains, and ultimately leading to variable clinical outcomes. Our findings might help to develop individual-based or subtype-specific diagnostic approaches and molecular classification of AD subtypes, which are prerequisites to developing AD therapeutic strategies. The subtype-specific Tau interactome map provides an exciting roadmap to explore new targets to slow down the disease progression in rpAD cases, and to explore new therapeutic targets and biomarkers, not only for AD but also for other related rapidly progressive dementias.

## AUTHOR CONTRIBUTIONS

Conceptualization and design of the study: AY, NY and IZ. Methodology: AY, NY, and IF. Data analysis and interpretation: AY, NY, MJ and IZ. Resources and materials: IZ and IF. Supervision: IZ and MJ. Writing original draft: AY and NY. Critical review and scientific input: IZ, MJ and IF. All authors revised and approved the final version of the manuscript.

## ACKNOWLEDGEMENTS

Open Access funding enabled and organized by Projekt DEAL.

## CONFLICT OF INTEREST STATEMENT

The authors declare no conflict of interest.

## DATA AVAILABILITY STATEMENT

All data generated or analysed during this study are included in the main article and its supplementary information files.

## ETHICS STATEMENT

All the procedures involving human brain samples were carried out following ethical regulations as stated in detail in the methods section.

## ORCID

Neelam Younas  <https://orcid.org/0000-0003-0421-5247>

Isidre Ferrer  <https://orcid.org/0000-0001-9888-8754>

## REFERENCES

1. Foiani MS, Woollacott IOC, Heller C, et al. Plasma tau is increased in frontotemporal dementia. *J Neurol Neurosurg Psychiatry*. 2018;89(8):804–807. doi:10.1136/jnnp-2017-317260
2. Ando K, Ferlini L, Suain V, et al. De novo MAPT mutation G335A causes severe brain atrophy, 3R and 4R PHF-tau pathology and early onset frontotemporal dementia. *Acta Neuropathol Commun*. 2020;8(1):94. doi:10.1186/s40478-020-00977-8
3. Devous MD, Fleisher AS, Pontecorvo MJ, et al. Relationships between cognition and neuropathological tau in Alzheimer's disease assessed by 18F Flortaucipir PET. *J Alzheimers Dis*. 2021;80(3):1091–1104. doi:10.3233/JAD-200808
4. Duara R, Barker W. Heterogeneity in Alzheimer's disease diagnosis and progression rates: implications for therapeutic trials. *Neurotherapeutics*. 2022;19(1):8–25. doi:10.1007/s13311-022-01185-z
5. Scheltens P, Blennow K, Breteler MMB, et al. Alzheimer's disease. *Lancet*. 2016. doi:10.1016/S0140-6736(15)01124-1
6. Podlesniy P, Llorens F, Puiggròs M, et al. Cerebrospinal fluid mitochondrial DNA in rapid and slow progressive forms of Alzheimer's disease. *Int J Mol Sci*. 2020;21(17):1–14. doi:10.3390/ijms21176298
7. Herden JM, Hermann P, Schmidt I, et al. Comparative evaluation of clinical and cerebrospinal fluid biomarker characteristics in rapidly and non-rapidly progressive Alzheimer's disease. *Alzheimer's Res Ther*. 2023;15(1):106. doi:10.1186/s13195-023-01249-y
8. Younas N, Zafar S, Shafiq M, et al. SFPQ and tau: critical factors contributing to rapid progression of Alzheimer's disease. *Acta Neuropathol*. 2020;140(3):317–339. doi:10.1007/s00401-020-02178-y
9. Schmidt C, Redyk K, Meissner B, et al. Clinical features of rapidly progressive Alzheimer's disease. *Dement Geriatr Cogn Disord*. 2010;29(4):371–378. doi:10.1159/000278692
10. Pillai JA, Appleby BS, Safar J, Leverenz JB. Rapidly progressive Alzheimer's disease in two distinct autopsy cohorts. *J Alzheimers Dis*. 2018;64(3):973–980. doi:10.3233/JAD-180155
11. Kim C, Haldiman T, Kang SG, et al. Distinct populations of highly potent TAU seed conformers in rapidly progressing Alzheimer's disease. *Sci Transl Med*. 2022;14(626):eabg0253. doi:10.1126/scitranslmed.abg0253
12. Schmidt C, Haik S, Satoh K, et al. Rapidly progressive Alzheimer's disease: a multicenter update. *J Alzheimers Dis*. 2012;30(4):751–756. doi:10.3233/JAD-2012-120007
13. Ba M, Li X, Ng KP, et al. The prevalence and biomarkers' characteristic of rapidly progressive Alzheimer's disease from the Alzheimer's disease neuroimaging initiative database. *Alzheimer's Dement Transl Res Clin Interv*. 2017;3(1):107–113. doi:10.1016/j.trci.2016.12.005
14. Hermann P, Haller P, Goebel S, et al. Total and phosphorylated cerebrospinal fluid tau in the differential diagnosis of sporadic Creutzfeldt-Jakob disease and rapidly progressive Alzheimer's disease. *Viruses*. 2022;14(2):276. doi:10.3390/v14020276
15. Qiang W, Yau WM, Lu JX, Collinge J, Tycko R. Structural variation in amyloid- $\beta$  fibrils from Alzheimer's disease clinical subtypes. *Nature*. 2017;541(7636):217–221. doi:10.1038/nature20814
16. Cohen ML, Kim C, Haldiman T, et al. Rapidly progressive Alzheimer's disease features distinct structures of amyloid- $\beta$ . *Brain*. 2015;138(4):1009–1022. doi:10.1093/BRAIN/AWV006
17. Liu H, Kim C, Haldiman T, et al. Distinct conformers of amyloid beta accumulate in the neocortex of patients with rapidly progressive Alzheimer's disease. *J Biol Chem*. 2021;297(5):101267. doi:10.1016/j.jbc.2021.101267
18. Bejanin A, Schonhaut DR, La Joie R, et al. Tau pathology and neurodegeneration contribute to cognitive impairment in Alzheimer's disease. *Brain*. 2017;140(12):3286–3300. doi:10.1093/brain/awx243
19. Dang M, Chen Q, Zhao X, et al. Tau as a biomarker of cognitive impairment and neuropsychiatric symptom in Alzheimer's disease. *Hum Brain Mapp*. 2022;44(2):327–340. doi:10.1002/hbm.26043
20. Mietelska-Porowska A, Wasik U, Goras M, Filipiek A, Niewiadomska G. Tau protein modifications and interactions: their role in function and dysfunction. *Int J Mol Sci*. 2014;15(3):4671–4713. doi:10.3390/ijms15034671
21. Mueller RL, Combs B, Alhadidy MM, Brady ST, Morfini GA, Kanaan NM. Tau: A Signaling Hub Protein. *Front Mol Neurosci*. 2021;14:647054. doi:10.3389/fnmol.2021.647054
22. Sinsky J, Pichlerova K, Hanes J. Tau protein interaction partners and their roles in Alzheimer's disease and other Tauopathies. *Int J Mol Sci*. 2021;22(17):9207. doi:10.3390/ijms22179207
23. Lippens G, Gigant B. Elucidating tau function and dysfunction in the era of cryo-EM. *J Biol Chem*. 2019. doi:10.1074/jbc.REV119.008031
24. Drummond E, Pires G, MacMurray C, et al. Phosphorylated tau interactome in the human Alzheimer's disease brain. *Brain*. 2020;143(9):2803–2817. doi:10.1093/brain/awaa223

25. Meier S, Bell M, Lyons DN, et al. Identification of novel tau interactions with endoplasmic reticulum proteins in Alzheimer's disease brain. *J Alzheimers Dis*. 2015;48(3):687-702. doi:[10.3233/JAD-150298](#)
26. Ayyadevara S, Balasubramaniam M, Parcon PA, et al. Proteins that mediate protein aggregation and cytotoxicity distinguish Alzheimer's hippocampus from normal controls. *Aging Cell*. 2016;15(5):924-939. doi:[10.1111/accel.12501](#)
27. Hsieh YC, Guo C, Yalamanchili HK, et al. Tau-mediated disruption of the spliceosome triggers cryptic RNA splicing and neurodegeneration in Alzheimer's disease. *Cell Rep*. 2019;29(2):301-316.e10. doi:[10.1016/j.celrep.2019.08.104](#)
28. Tracy TE, Madero-Pérez J, Swaney DL, et al. Tau interactome maps synaptic and mitochondrial processes associated with neurodegeneration. *Cell*. 2022;185(4):712-728.e14. doi:[10.1016/j.cell.2021.12.041](#)
29. Gunawardana CG, Mehrabian M, Wang X, et al. The human tau interactome: binding to the ribonucleoproteome, and impaired binding of the proline-to-leucine mutant at position 301 (P301L) to chaperones and the proteasome. *Mol Cell Proteomics*. 2015;14(11):3000-3014. doi:[10.1074/mcp.M115.050724](#)
30. Wang X, Williams D, Müller I, et al. Tau interactome analyses in CRISPR-Cas9 engineered neuronal cells reveal ATPase-dependent binding of wild-type but not P301L tau to non-muscle myosins. *Sci Rep*. 2019;9(1):1-21. doi:[10.1038/s41598-019-52543-5](#)
31. García-Esparcia P, Hernández-Ortega K, Koneti A, et al. Altered machinery of protein synthesis is region- and stage-dependent and is associated with  $\alpha$ -synuclein oligomers in Parkinson's disease. *Acta Neuropathol Commun*. 2015;3(1):76. doi:[10.1186/s40478-015-0257-4](#)
32. Schmidt C, Wolff M, Weitz M, Bartlau T, Korth C, Zerr I. Rapidly progressive Alzheimer disease. *Arch Neurol*. 2011;68(9):1124. doi:[10.1001/archneurol.2011.189](#)
33. Tyanova S, Cox J. Perseus: a bioinformatics platform for integrative analysis of proteomics data in cancer research. *Methods Mol Biol*. 2018. doi:[10.1007/978-1-4939-7493-1\\_7](#)
34. Tyanova S, Temu T, Sinitcyn P, et al. The Perseus computational platform for comprehensive analysis of (prote)omics data. *Nat Methods*. 2016;13(9):731-740. doi:[10.1038/nmeth.3901](#)
35. Zafar S, Younas N, Sheikh N, et al. Cytoskeleton-associated risk modifiers involved in early and rapid progression of sporadic Creutzfeldt-Jakob disease. *Mol Neurobiol*. 2018;55(5):4009-4029. doi:[10.1007/s12035-017-0589-0](#)
36. Muntel J, Gandhi T, Verbeke L, et al. Surpassing 10 000 identified and quantified proteins in a single run by optimizing current LC-MS instrumentation and data analysis strategy. *Mol Omi*. 2019;15(5):348-360. doi:[10.1039/c9mo00082h](#)
37. Bruderer R, Bernhardt OM, Gandhi T, et al. Extending the limits of quantitative proteome profiling with data-independent acquisition and application to acetaminophen-treated three-dimensional liver microtissues. *Mol Cell Proteomics*. 2015;14(5). doi:[10.1074/mcp.M114.044305](#)
38. Zou C, Su L, Pan M, et al. Exploration of novel biomarkers in Alzheimer's disease based on four diagnostic models. *Front Aging Neurosci*. 2023;15:1079433. doi:[10.3389/fnagi.2023.1079433](#)
39. Guix FX, Ill-Raga G, Bravo R, et al. Amyloid-dependent triosephosphate isomerase nitrotyrosination induces glycation and tau fibrillation. *Brain*. 2009;132(5):1335-1345. doi:[10.1093/brain/awp023](#)
40. Rocha S, Freitas A, Guimaraes SC, Vitorino R, Aroso M, Gomez-Lazaro M. Biological implications of differential expression of mitochondrial-shaping proteins in Parkinson's disease. *Antioxidants*. 2018;7(1). doi:[10.3390/antiox7010001](#)
41. Kanyenda LJ, Verdile G, Boulous S, et al. The dynamics of CD147 in Alzheimer's disease development and pathology. *J Alzheimers Dis*. 2011;26(4):593-605. doi:[10.3233/JAD-2011-110584](#)
42. Adav SS, Park JE, Sze SK. Quantitative profiling brain proteomes revealed mitochondrial dysfunction in Alzheimer's disease. *Mol Brain*. 2019;12(1):8. doi:[10.1186/s13041-019-0430-y](#)
43. Gui H, Gong Q, Jiang J, Liu M, Li H. Identification of the hub genes in Alzheimer's disease. *Comput Math Methods Med*. 2021;2021:6329041. doi:[10.1155/2021/6329041](#)
44. Brooks WM, Lynch PJ, Ingle CC, et al. Gene expression profiles of metabolic enzyme transcripts in Alzheimer's disease. *Brain Res*. 2007;1127:127-135. doi:[10.1016/j.brainres.2006.09.106](#)
45. Liu L, Wu Q, Zhong W, et al. Microarray analysis of differential gene expression in Alzheimer's disease identifies potential biomarkers with diagnostic value. *Med Sci Monit*. 2020;26:e919249. doi:[10.12659/MSM.919249](#)
46. Wang H, Dey KK, Chen PC, et al. Integrated analysis of ultra-deep proteomes in cortex, cerebrospinal fluid and serum reveals a mitochondrial signature in Alzheimer's disease. *Mol Neurodegener*. 2020;15(1):43. doi:[10.1186/s13024-020-00384-6](#)
47. Sinsky J, Majerova P, Kovac A, Kotlyar M, Jurisica I, Hanes J. Physiological tau Interactome in brain and its link to Tauopathies. *J Proteome Res*. 2020;19(6):2429-2442. doi:[10.1021/acs.jproteome.0c00137](#)
48. Gauthier-Kemper A, Alonso MS, Sündermann F, et al. Annexins A2 and A6 interact with the extreme N terminus of tau and thereby contribute to tau's axonal localization. *J Biol Chem*. 2018. doi:[10.1074/jbc.RA117.000490](#)
49. Shafiq M, Zafar S, Younas N, et al. Prion protein oligomers cause neuronal cytoskeletal damage in rapidly progressive Alzheimer's disease. *Mol Neurodegener*. 2021;16(1):11. doi:[10.1186/s13024-021-00422-x](#)
50. Yagensky O, Kohansai-Nodehi M, Gunaseeian S, et al. Increased expression of heme-binding protein 1 early in Alzheimer's disease is linked to neurotoxicity. *Elife*. 2019;8. doi:[10.7554/eLife.47498](#)
51. Drummond E, Nayak S, Faustin A, et al. Proteomic differences in amyloid plaques in rapidly progressive and sporadic Alzheimer's disease. *Acta Neuropathol*. 2017;133(6):933-954. doi:[10.1007/s00401-017-1691-0](#)
52. Rubin M. Do p values lose their meaning in exploratory analyses? It depends how you define the familywise error rate. *Rev Gen Psychol*. 2017;21(3):269-275. doi:[10.1037/gpr0000123](#)
53. Liao Y, Wang J, Jaehnig EJ, Shi Z, Zhang B. WebGestalt 2019: gene set analysis toolkit with revamped UIs and APIs. *Nucleic Acids Res*. 2019;47(W1):W199-W205. doi:[10.1093/nar/gkz401](#)
54. Abreha MH, Dammer EB, Ping L, et al. Quantitative analysis of the brain Ubiquitylome in Alzheimer's disease. *Proteomics*. 2018;18(20):e1800108. doi:[10.1002/pmic.201800108](#)
55. Caldera M, Buphamalai P, Müller F, Menche J. Interactome-based approaches to human disease. *Curr Opin Syst Biol*. 2017;3(June):88-94. doi:[10.1016/j.coisb.2017.04.015](#)
56. Kavanagh T, Halder A, Drummond E. Tau interactome and RNA binding proteins in neurodegenerative diseases. *Mol Neurodegener*. 2022;17(1):66. doi:[10.1186/s13024-022-00572-6](#)
57. Goode BL, Chau M, Denis PE, Feinstein SC. Structural and functional differences between 3-repeat and 4-repeat tau isoforms: implications for normal tau function and the onset of neurodegenerative disease. *J Biol Chem*. 2000. doi:[10.1074/jbc.M007489200](#)
58. Alquezar C, Arya S, Kao AW. Tau post-translational modifications: dynamic transformers of tau function, degradation, and aggregation. *Front Neurol*. 2021;11:595532. doi:[10.3389/fneur.2020.595532](#)
59. Vogel JW, Young AL, Oxtoby NP, et al. Four distinct trajectories of tau deposition identified in Alzheimer's disease. *Nat Med*. 2021;27(5):871-881. doi:[10.1038/s41591-021-01309-6](#)
60. Robbins M, Clayton E, Kaminski Schierle GS. Synaptic tau: a pathological or physiological phenomenon? *Acta Neuropathol Commun*. 2021;9(1):149. doi:[10.1186/s40478-021-01246-y](#)

61. Adams JN, Lockhart SN, Li L, Jagust WJ. Relationships between tau and glucose metabolism reflect Alzheimer's disease pathology in cognitively normal older adults. *Cereb Cortex*. 2019;29(5):1997-2009. doi:[10.1093/cercor/bhy078](https://doi.org/10.1093/cercor/bhy078)
62. Behl T, Kaur D, Sehgal A, et al. Exploring the potential role of rab5 protein in endo-lysosomal impairment in Alzheimer's disease. *Biomed Pharmacother*. 2022;148:112773. doi:[10.1016/j.biopha.2022.112773](https://doi.org/10.1016/j.biopha.2022.112773)
63. Amorim JA, Canas PM, Tomé AR, et al. Mitochondria in excitatory and inhibitory synapses have similar susceptibility to amyloid- $\beta$  peptides modeling Alzheimer's disease. *J Alzheimers Dis*. 2017;60(2):525-536. doi:[10.3233/JAD-170356](https://doi.org/10.3233/JAD-170356)
64. Goleva T, Rogov A, Zvyagilskaya R. Alzheimer's disease: molecular hallmarks and yeast models. *J Alzheimers Dis Park*. 2017;07(06). doi:[10.4172/2161-0460.1000394](https://doi.org/10.4172/2161-0460.1000394)
65. Guedes-Dias P, Holzbaur ELF. Axonal transport: driving synaptic function. *Science* (80-). 2019;366(6462). doi:[10.1126/science.aaw9997](https://doi.org/10.1126/science.aaw9997)
66. Balabanian L, Berger CL, Hendricks AG. Tau differentially regulates the dynamic localization of early endosomes and lysosomes. *Biophys J*. 2020;118(3):350a. doi:[10.1016/j.bpj.2019.11.2019](https://doi.org/10.1016/j.bpj.2019.11.2019)
67. Saito ER, Miller JB, Harari O, et al. Alzheimer's disease alters oligodendrocytic glycolytic and ketolytic gene expression. *Alzheimers Dement*. 2021;17(9):1474-1486. doi:[10.1002/alz.12310](https://doi.org/10.1002/alz.12310)
68. Davison EJ, Pennington K, Hung CC, et al. Proteomic analysis of increased Parkin expression and its interactants provides evidence for a role in modulation of mitochondrial function. *Proteomics*. 2009;9(18):4284-4297. doi:[10.1002/pmic.200900126](https://doi.org/10.1002/pmic.200900126)
69. Demonbreun AR, Bogdanovic E, Vaught LA, et al. A conserved annexin A6-mediated membrane repair mechanism in muscle, heart, and nerve. *JCI Insight*. 2022;7(14). doi:[10.1172/jci.insight.158107](https://doi.org/10.1172/jci.insight.158107)
70. Bin XY, Liu R, Wang XY, et al. COX5A plays a vital role in memory impairment associated with brain aging via the BDNF/ERK1/2 signaling pathway. *Front Aging Neurosci*. 2020;12:215. doi:[10.3389/fnagi.2020.00215](https://doi.org/10.3389/fnagi.2020.00215)
71. Lunnon K, Keohane A, Pidsley R, et al. Mitochondrial genes are altered in blood early in Alzheimer's disease. *Neurobiol Aging*. 2017;53:36-47. doi:[10.1016/j.neurobiolaging.2016.12.029](https://doi.org/10.1016/j.neurobiolaging.2016.12.029)
72. Patel VP, Chu CT. Nuclear transport, oxidative stress, and neurodegeneration. *Int J Clin Exp Pathol*. 2011.
73. Sheffield LG, Miskiewicz HB, Tannenbaum LB, Mirra SS. Nuclear pore complex proteins in Alzheimer disease. *J Neuropathol Exp Neurol*. 2006;65(1):45-54. doi:[10.1097/01.jnen.0000195939.40410.08](https://doi.org/10.1097/01.jnen.0000195939.40410.08)
74. Betters RK, Luhmann E, Gottschalk AC, et al. Characterization of the tau Interactome in human brain reveals isoform-dependent interaction with 14-3-3 family proteins. *eNeuro*. 2023;10(3):ENEURO.0503-22.2023. doi:[10.1523/ENEURO.0503-22.2023](https://doi.org/10.1523/ENEURO.0503-22.2023)
75. Wang Q, Woltjer RL, Cimino PJ, et al. Proteomic analysis of neurofibrillary tangles in Alzheimer disease identifies GAPDH as a detergent-insoluble paired helical filament tau binding protein. *FASEB j*. 2005;19(7):1-12. doi:[10.1096/fj.04-3210fje](https://doi.org/10.1096/fj.04-3210fje)

## SUPPORTING INFORMATION

Additional supporting information can be found online in the Supporting Information section at the end of this article.

**How to cite this article:** Younas A, Younas N, Iqbal MJ, Ferrer I, Zerr I. Comparative interactome mapping of Tau-protein in classical and rapidly progressive Alzheimer's disease identifies subtype-specific pathways. *Neuropathol Appl Neurobiol*. 2024;50(1):e12964. doi:[10.1111/nan.12964](https://doi.org/10.1111/nan.12964)